Evaluation of COAMPS Forecasts of Coastal Stratus Using Satellite Microphysical Retrievals and Aircraft Measurements

MELANIE A. WETZEL,* WILLIAM T. THOMPSON,+ GABOR VALI,# STEVEN K. CHAI,* TRACY HAACK,+ MARCIN J. SZUMOWSKI,* AND ROBERT KELLY#

*Desert Research Institute, Reno, Nevada
+Naval Research Laboratory, Monterey, California
#University of Wyoming, Laramie, Wyoming

(Manuscript received 13 September 2000, in final form 15 May 2000)

ABSTRACT

A field project was carried out offshore of central Oregon during August 1999 to evaluate mesoscale model simulations of coastal stratiform cloud layers. Procedures for mapping cloud physical parameters such as cloud optical depth, droplet effective radius, and liquid water path retrieved from Geostationary Operational Environmental Satellite (GOES) Imager multichannel data were developed and implemented. Aircraft measurements by the University of Wyoming provided in situ verification for the satellite retrieval parameters and for the forecast model simulations of the U.S. Navy's nonhydrostatic mesoscale prediction system, the Coupled Ocean/Atmosphere Mesoscale Prediction System (COAMPS). Case studies show that the satellite retrieval methods are valid within the range of uncertainty associated with aircraft measurements of the microphysical parameters and demonstrate how the gridded cloud parameters retrieved from satellite data can be utilized for mesoscale model verification. Satellite-derived products with applications to forecasting, such as temporal trends and composites of droplet size and liquid water path, are also discussed.

1. Introduction

Many observational studies have been conducted over recent decades to characterize the structure of marine stratus (Noonkester 1984; Minnis et al. 1992; Albrecht et al. 1994). Prediction of boundary layer cloudiness is a difficult aspect of marine forecasting due to the multiple scales of boundary layer dynamic processes and the lack of observations in many oceanic and coastal regions. The ability to correctly forecast cloud-layer evolution is strongly tied to the accuracy with which a model simulates the vertical profile of liquid water. This is due to the influence of the cloud water profile on radiative heating or cooling, entrainment effects, and microphysical processes (Oliver et al. 1978; Telford and Chai 1984, 1993; Thompson et al. 1997). During the nocturnal regime, turbulence generated by longwave cooling is generally sufficient to produce mixing from the surface to the top of the marine boundary layer (MBL). However, net radiative cooling during the day may be insufficient to promote mixing through the entire depth of the MBL and the cloud layer may become decoupled from the subcloud layer (Tjernstrom and Koracin 1995). Diurnal cycles in cloud structure respond to interactions between cloud physical and dynamical processes. Wai (1991) isolated three mechanisms leading to stratus dissipation: 1) advection of dry air into the MBL, 2) absorption of solar radiation, and 3) mesoscale variations in the velocity field, leading to inhomogeneities in the cloud layer. Cloud-top entrainment instability was shown by Tag and Payne (1987) to be important in stratus breakup. Each of these processes is sensitive to the distribution of cloud liquid water within the MBL.

The observed diurnal patterns and mesoscale variability of stratus point to the need for satellite remote sensing methods that can be used to augment numerical simulation models as both forecast verification data and supplemental information for short-term forecast products. Multichannel satellite remote sensing can provide near-continuous mapping of the distribution of stratus cloud layers (Lee et al. 1997). Remote sensing of cloud microphysical parameters also has the potential to significantly improve monitoring and understanding of the physical mechanisms that cause stratus development and dissipation (Greenwald and Christopher 1999). This paper demonstrates satellite remote sensing to map cloud liquid water path and other microphysical parameters for intercomparison with mesoscale model simulations of stratus layers. Section 2 describes a field program that was conducted for the purpose of evaluating remote sensing retrieval methods for cloud microphysical pa-

Corresponding author address: Dr. Melanie A. Wetzel, Desert Research Institute, 2215 Raggio Parkway, Reno, NV 89512.
E-mail: wetzel@dri.edu

rameters and their use in validation of the Naval Research Laboratory (NRL) Coupled Ocean/Atmosphere Mesoscale Prediction System (COAMPS) model simulations. The satellite analysis methods are discussed in section 3, with focus on the use of aircraft data to verify the remote sensing retrieval results. Satellite–model intercomparisons are presented in section 4, which is followed by concluding discussion in section 5.

2. COSAT '99 project

A collaborative field program, the COAMPS Operational Satellite and Aircraft Test (COSAT) was designed to demonstrate methods for integrating satellite remote sensing retrieval products with mesoscale model simulations of coastal stratus cloud layers. Numerical simulations from the U.S. Navy's COAMPS model were compared to corresponding satellite and aircraft observations. Scientists from the Desert Research Institute (DRI), NRL, the University of Wyoming (UW), and Oregon State University participated in the field experiment during the period of 4–29 August 1999. Operations were based at the Corvallis airport in west-central Oregon. The UW King Air instrumented aircraft was deployed from the Corvallis airport for several flights into the marine stratus and stratocumulus layers offshore.

Satellite remote sensing analysis was conducted at the field site by DRI scientists using digital processing and implementation of radiative transfer retrieval methods described in the next section. COAMPS parameter fields produced by NRL scientists provided modeling support and forecast guidance in near–real time. Oregon State University was also running the Advanced Regional Prediction System mesoscale model for the region during this period. The individual components of the field program each provided data for use in flight planning and case analysis.

3. Satellite retrievals

a. Methodology

Satellite remote sensing retrieval methods using multispectral radiance data from the National Oceanographic and Atmospheric Administration (NOAA) Geostationary Operational Environmental Satellite (GOES) Imager and the Advanced Very High Resolution Radiometer (AVHRR) instruments were used for estimation of cloud droplet size and optical depth (Wetzel et al. 1996; Wetzel and Stowe 1999). Satellite data for the operational field program in August 1999 were obtained from the *GOES-10* imager, primarily the visible channel 1 (0.57–0.72 μm), the near-infrared channel 2 (3.78–4.03 μm), and the thermal infrared window channel 4 (10.2–11.2 μm). Cloudy pixels were limited to an equivalent channel 4 cloud-top temperature > 0°C, and subjective image analysis for the case studies was used to eliminate any time periods where high clouds obscured the boundary layer clouds. The cloud optical depth (τ) and cloud droplet effective radius (R_e) were found by interpolation from the observed satellite pixel reflectances in the visible and near-infrared channels to arrays of precalculated radiative transfer model reflectances (Wetzel and Stowe 1999). The optical depth is expressed as

$$\tau = \int_{z1}^{z2} \sigma_{\text{ext}}\, dz, \tag{1}$$

where σ_{ext} is the volume extinction coefficient for the cloud droplet distribution and dz is the vertical increment for the integration from cloud base ($z1$) to cloud top ($z2$). The effective radius is defined as

$$R_e = \int_0^\infty r^3 n(r)\, dr \Big/ \int_0^\infty r^2 n(r)\, dr, \tag{2}$$

where r is droplet radius and $n(r)$ is the size distribution for the droplet population.

Cubic spline interpolation was implemented to estimate cloud optical depth from visible reflectances, then to retrieve cloud droplet effective radius from the near-infrared reflectances for each cloudy pixel. The thermal infrared channel data were used to subtract the thermal emission component from the emissivity-adjusted near-infrared radiance, using a method similar to that of Kaufman and Nakajima (1993). Analysis of Miller (2001) using data obtained during a solar eclipse suggests that emissivity correction produces 3.9-μm reflectance values with an error of approximately 15% or less, for clouds of sufficient optical thickness (e.g., when 3.9-μm reflectance >0.1). Satellite retrievals of optical depth have an uncertainty of approximately $\pm 20\%$ for marine stratus layers (Platnick and Valero 1995). Sensitivity tests on calculated reflectances for stratus clouds with vertically increasing droplet size (Wetzel and Vonder Haar 1991) indicate that for the conditions of R_e and liquid water content profiles described here, the satellite-estimated R_e represents the actual R_e in the upper 100 m of cloud within 1–2 μm (equivalent to $\pm 5\%$–20% of R_e for the conditions found in this study). These uncertainties are applied to the retrievals discussed in later sections.

The Discrete Ordinates model (DISORT; Stamnes et al. 1988) was used to produce tabular reflectance data for a wide range of R_e, τ, and solar/viewing geometry conditions, covering all possible image pixel viewing angles and cloud types. Cloud optical properties were determined from a narrowband parameterization based on Mie theory using the gamma size distribution. Gas absorption coefficients using the exponential sum fitting technique were derived for water vapor, carbon dioxide, ozone, and oxygen (Meier et al. 1997). The satellite channel filter functions for *GOES-10* were applied in the model calculations of band radiances. The following

equation (Han et al. 1995) provides the estimates of cloud liquid water path (LWP) using the optical depth and effective radius parameters derived from the satellite retrievals:

$$\mathrm{LWP} = 4\rho_w \tau R_e / 3Q_{\mathrm{ext}}, \quad (3)$$

where LWP has units (g m^{-2}), ρ_w is the density of liquid water (10^6 g m^{-3}), τ is nondimensional, effective radius (R_e) is expressed as microns, and the average extinction efficiency for the droplet size distribution (Q_{ext}) is approximately 2 (nondimensional). This parameterization assumes that the radiative signature represented by the visible and near-infrared radiances of the cloud is dominated by reflectance from the cloud-top layer.

In the marine stratus layers characterized in this study, cloud liquid water content typically increases nearly linearly with height. The droplet-effective radius also increases with height to cloud top and there is little transmission from below cloud, so the above assumption will generally hold true. However, the satellite-derived R_e value more closely matches the average value in the top 50–100 m of the cloud (Wetzel and Vonder Haar 1991) than that at immediate cloud top. Thus, the satellite-derived LWP value can be expected to be slightly less than LWP calculated by numerical integration using aircraft vertical profiles of liquid water content. The exact correspondence between satellite- and aircraft-derived LWP values also is influenced by cloud horizontal inhomogeneity, which influences both the calculations based on the aircraft instruments along their sampling path and the multichannel radiances observed by the satellite sensor.

b. Validation of retrieved parameters

1) AIRCRAFT INSTRUMENTATION

Measurements obtained by the UW King Air were utilized for detailed analysis of cloud structure as well as for vertical profiles of cloud droplet size and liquid water content. Multiple sensor systems recorded 1-Hz (and higher frequency) thermodynamic, air motion, and microphysical parameters (Vali et al. 1998). The Particle Measuring Systems Forward Scattering Spectrometer Probe (FSSP), Gerber Particulate Volume Monitor (PVM), and Droplet Measurement Technologies (DMT) hot-wire liquid water content (LWC-100) probes on the aircraft provided liquid water content and droplet size data for use in the intercomparison with model- and satellite-derived estimates. Gerber (1996) found agreement within 10%–15% between liquid water contents obtained from hot-wire probes and the PVM instrument. Similar accuracies are reported for droplet sizes obtained from the FSSP instruments (Vali et al. 1998), and agreement within 18%–20% is reported between liquid water contents derived from hot-wire probes and the FSSP (Paluch et al. 1996; Vali et al. 1998).

Summary data for aircraft parameters such as cloud R_e, liquid water content, and temperature were selected from ascent/descent flight legs as well as constant-altitude segments in order to evaluate the vertical profiles and horizontal structure of the cloud layers. Case study datasets were obtained for 19 different aircraft sampling flights during the August 1999 field project. The subset of flight periods presented in this paper was selected based on the availability of simultaneous satellite and aircraft datasets.

2) ANALYSIS OF RESULTS FOR 17 AUGUST CASE

Figure 1a shows the study region with the cloud distribution and a flight track for the case study day of 17 August 1999. Figure 1b shows the corresponding LWP distribution at 1630 UTC. Ascent/descent sampling profiles were obtained by the King Air during that time period, and the satellite pixels used for comparison were those directly matching the path of the aircraft. Figure 2 portrays the vertical profiles of cloud liquid water content obtained by the DMT, FSSP, and PVM instruments for a flight segment obtained during 1631–1634 UTC on 17 August, which took place near the center of the overall flight trajectory (near 43.7°N, 124.8°W in Fig. 1a). As is evident from this figure, the variation in liquid water content and hence the vertically integrated LWP values that are estimated from aircraft sensors can differ significantly. The range in values for measured LWP is 0.059–0.107 kg m^{-2}, and results of sampling by the hot-wire probe (DMT), which is the most commonly used type of liquid water content sensor, fall in the middle of that range. The satellite-estimated LWP for the image pixels located along the aircraft profile flight trajectory ranges from 0.058 to 0.064 kg m^{-2}. The FSSP and PVM measurements of R_e at cloud top were 11–13 μm while the range of satellite-derived R_e values across the pixels representing the aircraft flight trajectory during this profile was 12–13 μm. This type of analysis for short flight segments corresponding to individual ascent or descent profiles was carried out over multiple days during the field program.

3) COMPOSITE RESULTS FOR MULTIPLE CASE STUDIES

The series of aircraft and satellite intercomparisons described above were analyzed for several image dates and times. Estimates of R_e obtained from the satellite retrieval method, and LWP obtained from the Han et al. (1995) parameterization, were mapped over the satellite image domain. Individual flight segments are directly matched by geographic location to the gridded and mapped satellite retrieval parameters for the closest available satellite image dataset (within 15 min). A list of aircraft- and satellite-derived values of effective radius and liquid water path for several flight segments is shown in Table 1. In the case of the satellite-derived parameters, the ranges of values are those found for the

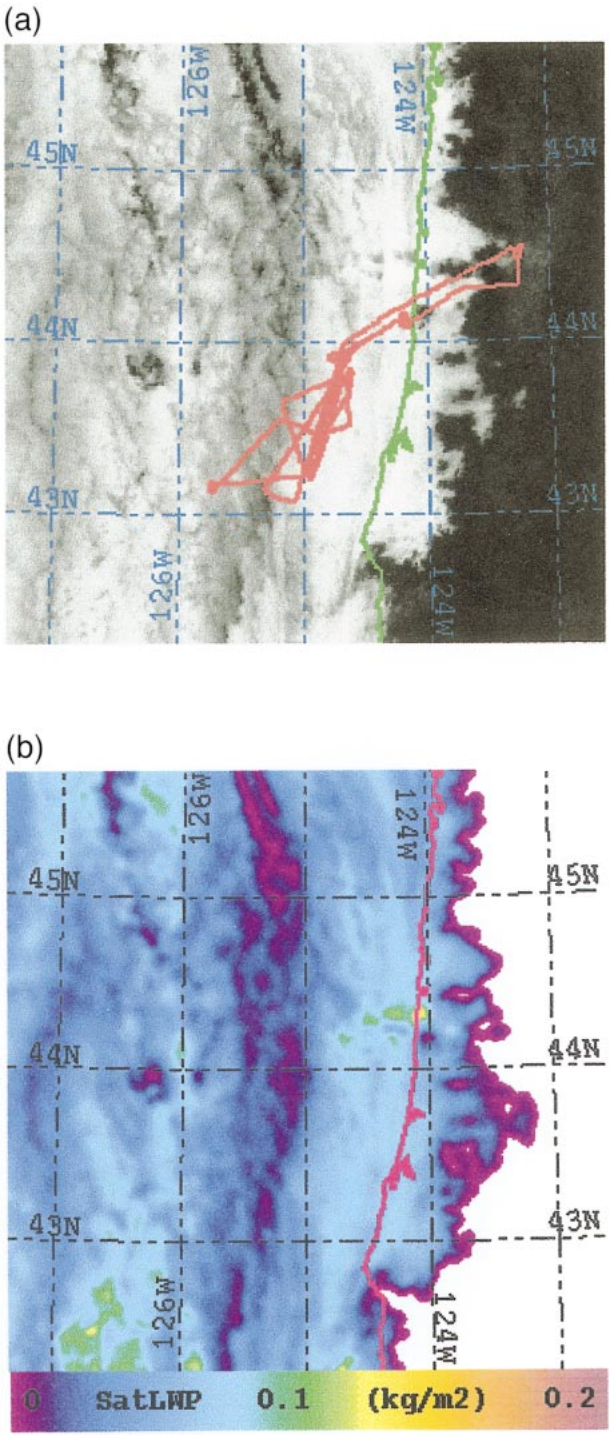

FIG. 1. (a) GOES visible image at 1630 UTC 17 Aug 1999, with graphic overlays of the flight track (red), lat–long grid (blue), and Oregon coastline (green). (b) GOES-derived cloud liquid water path (kg m^{-2}) at 1630 UTC 17 Aug 1999, with graphic overlays of the lat–long grid (black) and the central Oregon coastline (red).

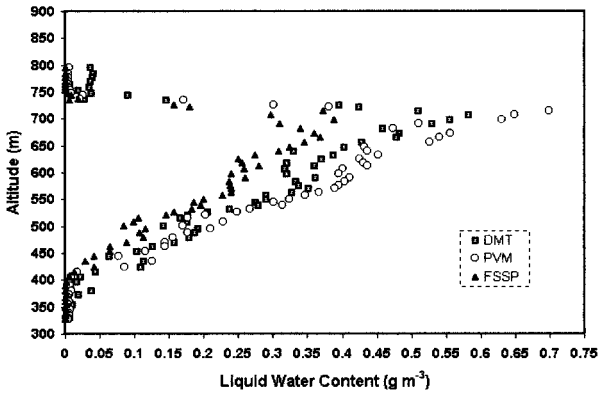

FIG. 2. Cloud LWC (g m^{-3}) from aircraft profiles on 17 Aug 1999 over the time period 1631–1634 UTC. Individual data points shown are 1-s averages of values obtained from the DMT (squares), PVM (circles), and FSSP (triangles) instruments.

image pixels collocated along the aircraft flight trajectory during the short-term ascent/descent profiles. These trajectories have durations of a few to several minutes of flight time. In the case of the aircraft-derived microphysical parameters, the ranges were obtained from measurements by different instruments. The R_e measurements were obtained simultaneously by the FSSP and PVM sensors, while the DMT, FSSP, and PVM sensors measured the liquid water content values used to derive the LWP values by vertical integration over the aircraft ascent or descent profile.

The effective radius values obtained from the analysis of the GOES satellite data vary from 8 to 16 μm for these case study days, as do the values measured by the in situ aircraft sensors. Variability in satellite-derived values of R_e along the aircraft sampling track during the profile data collection segments is ≤ 2 μm, and the magnitudes and ranges of R_e match those determined from the aircraft probes (Table 1), within the 10%–20% uncertainty expected for these instruments as discussed earlier. Liquid water path values derived from the sat-

TABLE 1. Aircraft- and satellite-derived values of effective radius (R_e) and liquid water path (LWP) for COSAT case studies in Aug 1999. The ranges of values correspond to variations between the various instruments available (for the aircraft data) and along the pixel sampling track matching the aircraft profile trajectory (for the satellite data).

Date	Time (UTC)	Satellite R_e (μm)	Aircraft R_e (μm)	Satellite LWP (kg m^{-2})	Aircraft LWP (kg m^{-2})
9 Aug	1700	8–9	8–9	0.018–0.028	0.044–0.061
9 Aug	1800	8–9	10	0.047–0.063	0.073–0.096
10 Aug	1600	10–11	10	0.058–0.063	0.101–0.148
10 Aug	1800	10	10	0.069–0.090	0.070–0.098
11 Aug	1600	15–16	12–16	0.052–0.076	0.054–0.063
11 Aug	1700	12–14	13–14	0.034–0.049	0.052–0.067
16 Aug	1630	11–12	13	0.026–0.047	0.061–0.093
16 Aug	1730	10–11	12	0.029–0.046	0.032–0.056
17 Aug	1600	10–11	10	0.022–0.026	0.029–0.050
17 Aug	1630	12–13	11–13	0.058–0.064	0.059–0.107

ellite datasets range between 0.018 and 0.090 kg m^{-2}, while aircraft sampling indicated the same flight profiles to have LWP in the range 0.029–0.148 kg m^{-2}. The range of LWP values obtained from the aircraft sensors for the individual profiles overlaps that derived from the satellite data analysis in most cases.

The results shown in Table 1 suggest a tendency for satellite underestimation of LWP by up to 0.05 kg m^{-2} for a few of the profiles. The underestimation may be caused by irregular vertical profiles of either R_e and LWC below cloud top, the presence of cumulus elements and other cloud structure inhomogeneity at cloud top, or improper geolocation of the aircraft path within the individual 4-km satellite pixels. The magnitudes of aircraft and satellite estimates of R_e and LWP are similar to those obtained for observational studies of California coastal stratus summarized for the First ISCCP (International Satellite Cloud Climatology Project) Regional Experiment-Stratus characterization program (Minnis et al. 1992).

Note that the values of aircraft-estimated LWP for 9–11 August shown in Table 1 are for specific short flight segments used for validation of the satellite retrieval method. For study of the spatial and temporal evolution of the LWP field, the satellite retrieval method was used to map LWP over the fine-mesh (inner) domain of the COAMPS model in the region where aircraft measurements were also available. The overall agreement in the variability and magnitudes of R_e and LWP demonstrates that the retrieval methods can be applied to mapping the distributions of these parameter fields for comparison with forecast model output, with attention to the evidence for a slight underestimation of LWP obtained from the satellite retrievals.

4. Satellite and model intercomparisons

a. Description of the COAMPS model

COAMPS is a three-dimensional nonhydrostatic forecasting model developed at NRL (Hodur 1997). The horizontal resolutions of the three nested domains used in this study were 81, 27, and 9 km. The bulk water cloud microphysics scheme follows Rutledge and Hobbs (1983). Output data for the 9-km grid resolution are used in this analysis. The model was run twice daily using a 12-h data assimilation update cycle, so that each forecast was initialized using a first-guess analysis from the previous 12-h forecast combined with current observational data using a multivariate optimum interpolation scheme. The data assimilation was continuous through the month of August 1999. Time-dependent external boundary conditions on the outer nest were supplied from analysis and forecast fields of the Navy Operational Global Atmospheric Prediction System (NOGAPS) model (Hogan and Rosmond 1991). A 36-h forecast was produced from the 0000 UTC run for flight-planning purposes. The 1200 UTC run produced a 12-h forecast in order to maintain the data assimilation cycle.

The Rutledge and Hobbs (1983) scheme features five prognostic equations for the following species of water substance: water vapor, cloud water, rainwater, cloud ice, and snow. Thirteen processes for conversion from one species to another are included. Of most interest in this study are conversions to and from water vapor and cloud water and the autoconversion of cloud water to rainwater. The autoconversion threshold is fairly high, such that the model produced rainwater only after attaining 1 g kg^{-1} liquid water mixing ratio and thus the model is unable to produce drizzle. The lack of this important sink of cloud water results in an overprediction of liquid water content.

COAMPS reproduces the observed strong cloud-top cooling over a shallow layer due to longwave radiative flux divergence. The Mellor and Yamada level-2.5 turbulence closure scheme (Mellor and Yamada 1982) responds to destabilization of the cloud top by producing large turbulence intensity, promoting entrainment, and strengthening the inversion. This tightly coupled, nonlinear interaction between clouds, radiation, and turbulence is critical in correctly modeling the evolution of marine stratus and stratocumulus (Oliver et al. 1978; Thompson et al. 1997). The COAMPS model was run in two modes; first using 30 vertical levels in the ''operational'' mode as was carried out for the real-time forecasting during the field project, and then using 45 levels in ''high resolution'' research mode, with 60-m vertical resolution in the lower levels (to 1600-m altitude).

The COAMPS model's sigma-level data, and the output fields closest in time to the aircraft observing period, were used for analysis. In the cloud microphysics scheme, water substances were divided into four categories: cloud water, rainwater, ice crystals, and snow. For purposes of comparison to satellite and aircraft data, liquid water path was derived by vertical integration of cloud water mixing ratio greater than 10^{-7} kg kg^{-1} between cloud base and cloud top, scaled for each layer from mixing ratio to liquid water content.

b. Case study of 9–11 August

Detailed analyses have been completed for several case studies including multiday sequences. A 3-day sequence of 9–11 August was selected due to the observed evolution of the boundary layer dynamic structure and cloudiness, as well as the availability of simultaneous satellite and aircraft datasets. The synoptic pattern was characterized by a weak surface trough over the western United States and an offshore high to the northwest of the project area, with passage of a weak upper-level trough across the northern Oregon coastal region during 10–11 August. Northerly winds create offshore flow over the coastal water due to the Coriolis force and thus lead to upwelling. The sea surface temperature is cooled

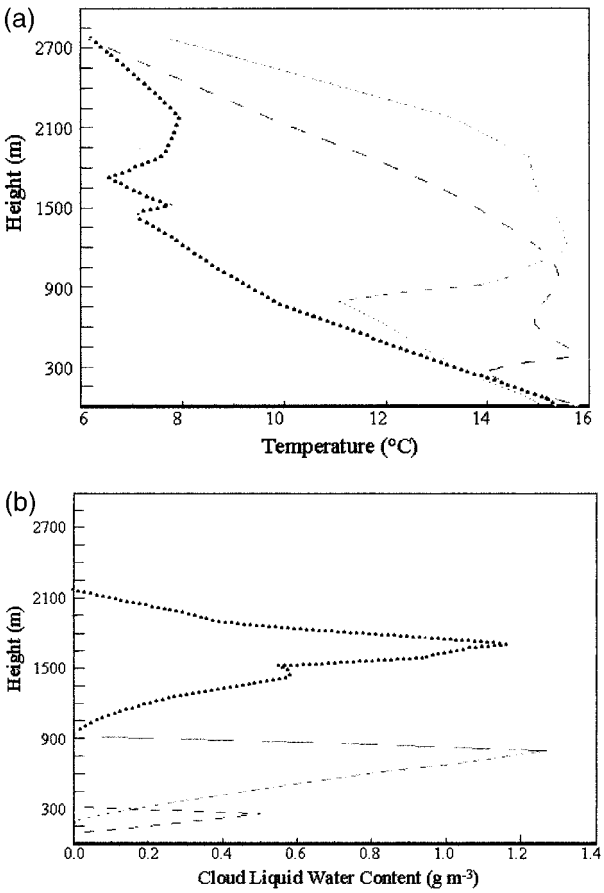

FIG. 3. COAMPS-predicted profiles of (a) temperature (°C), and (b) cloud LWC (g m^{-3}) on 9 (dashed), 10 (solid), and 11 Aug (dotted) for gridpoint profiles taken in the region of aircraft sampling.

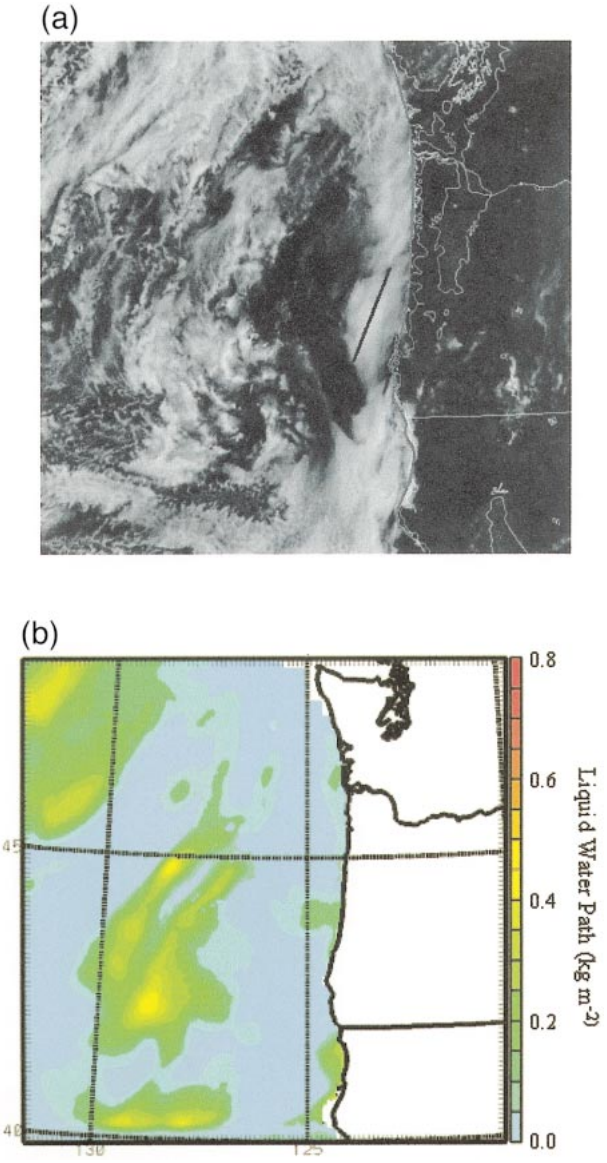

FIG. 4. (a) GOES visible satellite image at 1800 UTC 9 Aug 1999, with graphic overlay (solid line along central Oregon coast) to indicate the general area of flight sampling. (b) COAMPS forecast of LWP (kg m^{-2}) over the ocean region of the model domain for 1800 UTC 9 Aug 1999 with overlay of lat–long grid.

below air temperature, which leads to the formation of a low-level inversion and marine stratus layers (Telford and Chai 1984).

Model forecasts of the temperature and cloud liquid water content for 9–11 August are shown in Figs. 3a and 3b, respectively, using gridpoint vertical profiles selected using the area of the aircraft sampling flights on each day. The areas of aircraft flights are graphic overlays on a sequence of visible satellite images from this period (Fig. 4a, Fig. 5a, and Fig. 6a). During this 3-day sequence, the cloud field underwent a transition from scattered thin stratus to banded, cellular stratocumulus.

Gridded fields of stratus LWP were produced from the model layer output (Fig. 4b, Fig. 5b, and Fig. 6b). LWP for the COAMPS model was calculated by vertical integration of cloud liquid water mixing ratio (q_l) over stratus layers from

$$\text{LWP} = \sum_{i=0}^{n} q_{l,i}\, dp_i/g, \tag{4}$$

for all model layers where $q_l > 10^{-7}$ kg kg^{-1} pressure difference is dp for each individual model layer (i) between the surface and the cloud top, and g is the gravitational constant.

Comparison of the visible satellite images and the model-generated LWP fields indicates overall agreement in the evolution of the cloud fields, beginning on 9 August (Fig. 4) with thin, patchy coastal stratus and deeper convection offshore (cloud region indicated near 44°N, 128°W in Fig. 4b); more widespread stratiform cover along the coast on 10 August (Fig. 5) with a clear area just south of the coastal protrusion in southern Oregon; and cellular bands extending southwestward

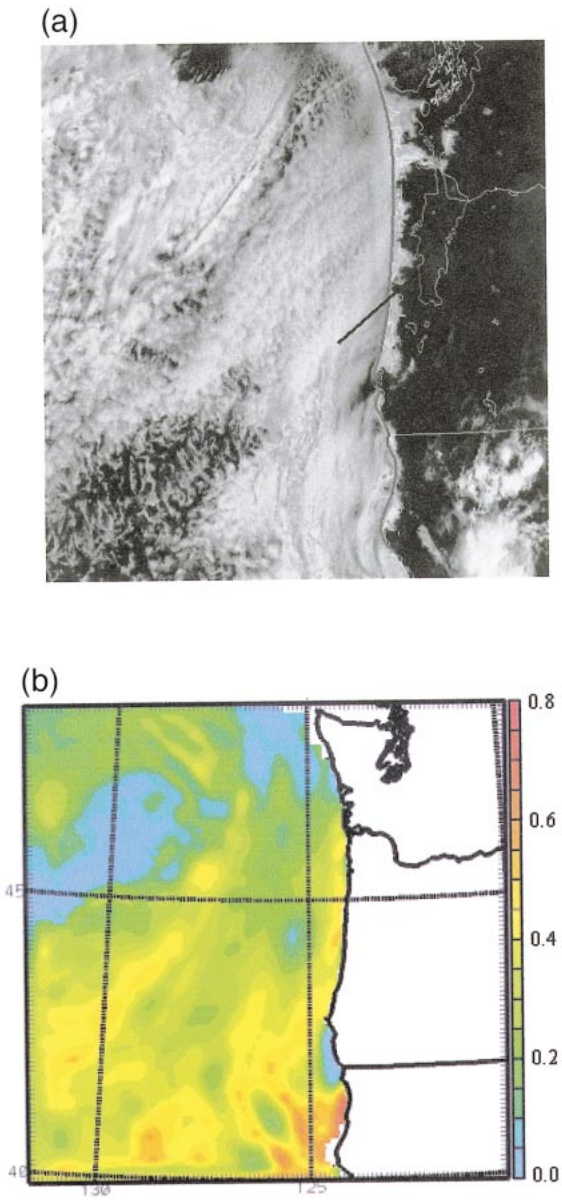

FIG. 5. (a) GOES visible satellite image at 1800 UTC 10 Aug 1999, with graphic overlay (solid line along central Oregon coast) to indicate the general area of flight sampling. (b) COAMPS forecast of LWP (kg m^{-2}) over the ocean region of the model domain for 1800 UTC 10 Aug 1999 with overlay of lat–long grid.

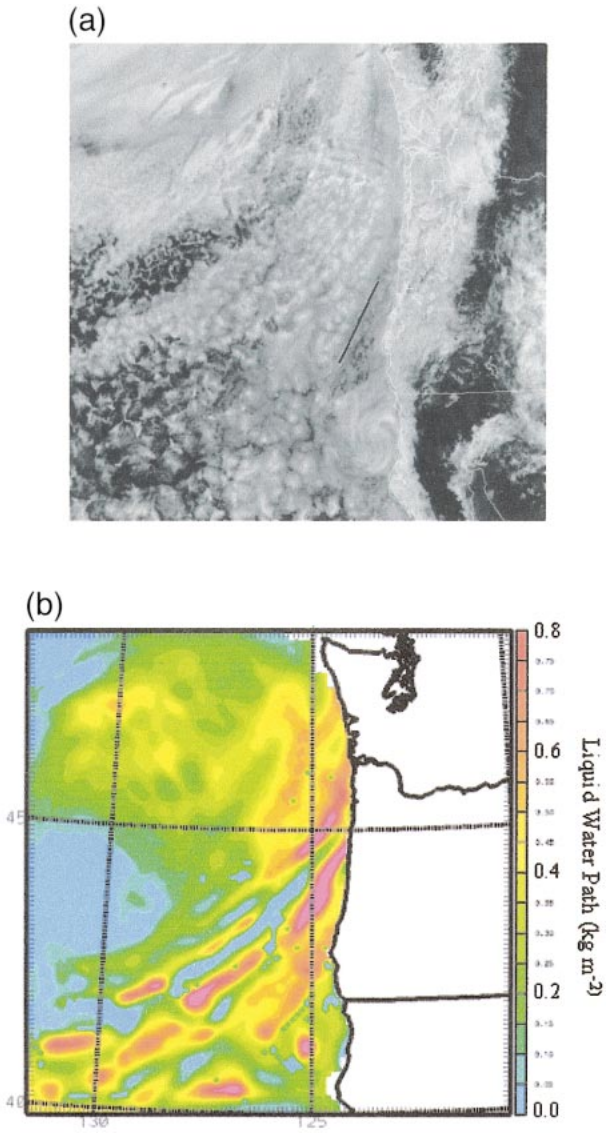

FIG. 6. (a) GOES visible satellite image at 1800 UTC 11 Aug 1999, with graphic overlay (solid line along central Oregon coast) to indicate the general area of flight sampling. (b) COAMPS forecast of LWP (kg m^{-2}) over the ocean region of the model domain for 1800 UTC 11 Aug 1999 with overlay of lat–long grid.

with a small vortex feature offshore of northern California on 11 August (Fig. 6).

Examination of the COAMPS predicted 3-hourly cross sections (not shown here) extending from the coast to 130°W (~500 km distance) and from the surface to 3 km indicates that the predicted MBL on 9 August was 300–500 m deep with scattered clouds. The clouds became more extensive during the period and by 0000 UTC 10 August they spanned the entire cross section. The MBL began to deepen rapidly at 30 h as the cloud thickness increased. By 36 h (1200 UTC 10 Aug), the mean boundary layer depth was predicted to be ~750 m and the cloud layer was uniformly 600 m in depth. The MBL continued to deepen over the next 12 h while the mean cloud thickness decreased and horizontal inhomogeneities developed in the field of cloud liquid water content. By 48 h (0000 UTC 11 Aug), the cloud layer was discontinuous with individual elements exhibiting vertical development, suggestive of a transition from stratus to stratocumulus. The inversion at the top of the MBL was predicted to reach an elevation of approximately 2 km with significant stratification in the upper part of the MBL both within the clouds and in clear areas between cloud.

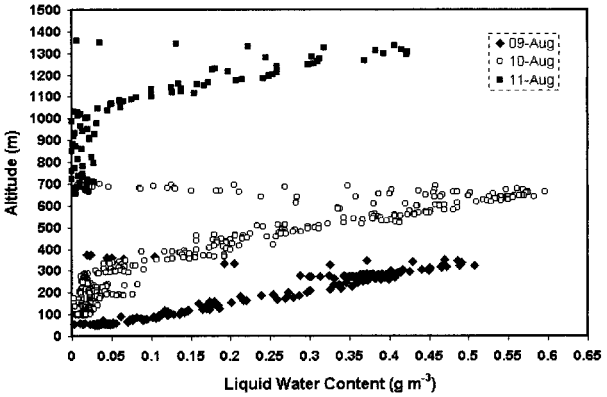

FIG. 7. Profiles of cloud LWC (g m^{-3}) on 9 (dashed), 10 (solid), and 11 Aug (dotted) for gridpoint profiles obtained by aircraft sampling using the DMT LWC-100 hot-wire probe.

Figure 7 presents aircraft-derived vertical profiles of cloud liquid water content for sampling areas matching the COAMPS profiles shown in Fig. 3b. The aircraft profiles suggest that while the model forecast of cloud water was somewhat underestimated on 9 August, the cloud liquid water path was significantly overestimated on 10 and 11 August. The cloud depth and height as well as the maximum liquid water content were larger in the model simulations than indicated by aircraft sampling. The satellite-derived gridded fields of LWP were produced to further examine these discrepancies. Figures 8–10 depict mesoscale analyses of satellite- and model-derived LWP for a 3-day time series of 9–11 August.

Figure 8a shows the satellite-derived LWP over the study area selected for detailed analysis of aircraft data. Maximum values of satellite-derived LWP were 0.05–0.1 kg m^{-2} for this time period. Figure 8b shows the 18-h forecast of vertically integrated cloud water path, valid at 1800 UTC on 9 August. The maximum LWP values for the patches of coastal stratus were in the range 0.1–0.2 kg m^{-2}. Figures 9a and 9b present the LWP fields for the satellite- and model-derived analyses, respectively, for 1800 UTC on 10 August. Each indicates a large increase in LWP from the previous day. The satellite-estimated LWP reached a maximum of approximately 0.15-kg m^{-2}, while the model produced maximum values near 0.5 kg m^{-2} on 10 August. However, note the similarity in the extent of coastal overrunning by the stratus layer, as well as the overall pattern of LWP maxima along the northern Oregon coastline and extending southwestward.

Figures 10a and 10b show the LWP fields for 1800 UTC on 11 August, each with large increases of LWP during the preceding 24 h, particularly located within the cloud bands extending southwestward across the coast into the offshore region. The model simulations produced significantly larger magnitudes of LWP (exceeding 1.0 kg m^{-2}) than those obtained from the satellite analyses (0.20 kg m^{-2}). Again in this case, there

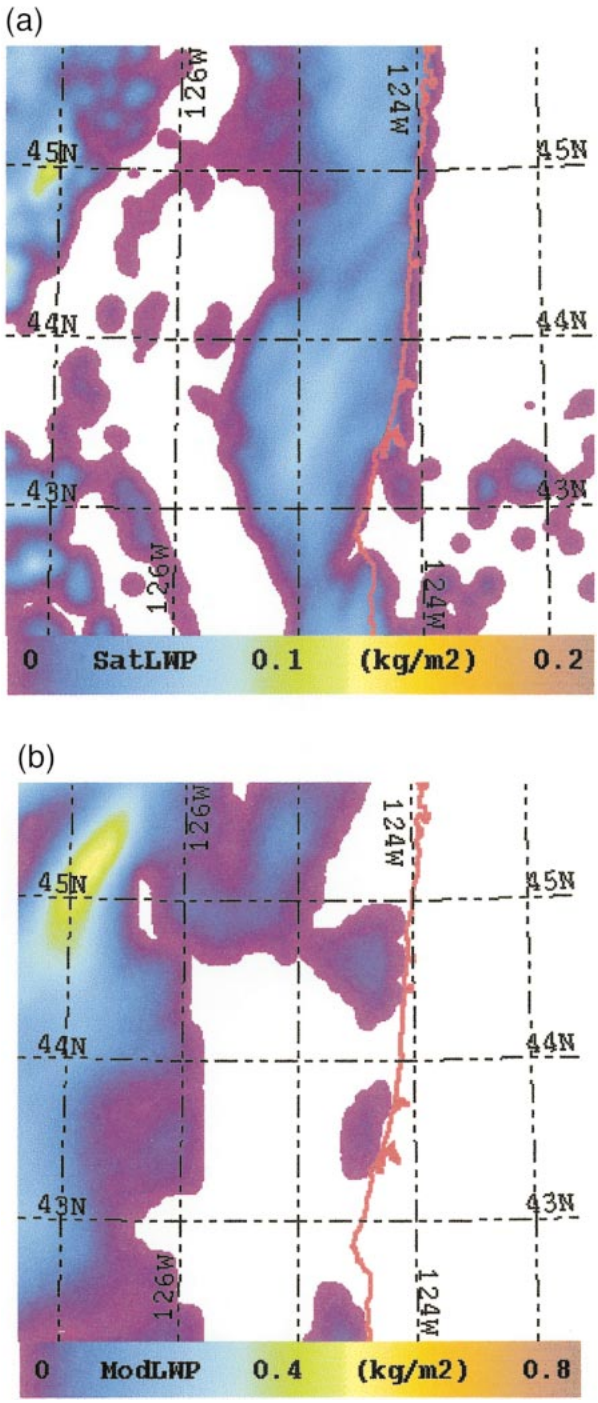

FIG. 8. (a) Satellite-estimated LWP (kg m^{-2}) and (b) COAMPS simulations of LWP (kg m^{-2}) at 1800 UTC 9 Aug for the study region, with graphic overlay of the lat–long grid.

is general agreement in the horizontal structure of the cloud field, including the extensive incursion of cloud on shore, and the orientation of the deep cloud bands.

In summary, the COAMPS forecasts captured the evolution of cloud structure and the trend toward increased LWP over the 3-day sequence, but overpredicted

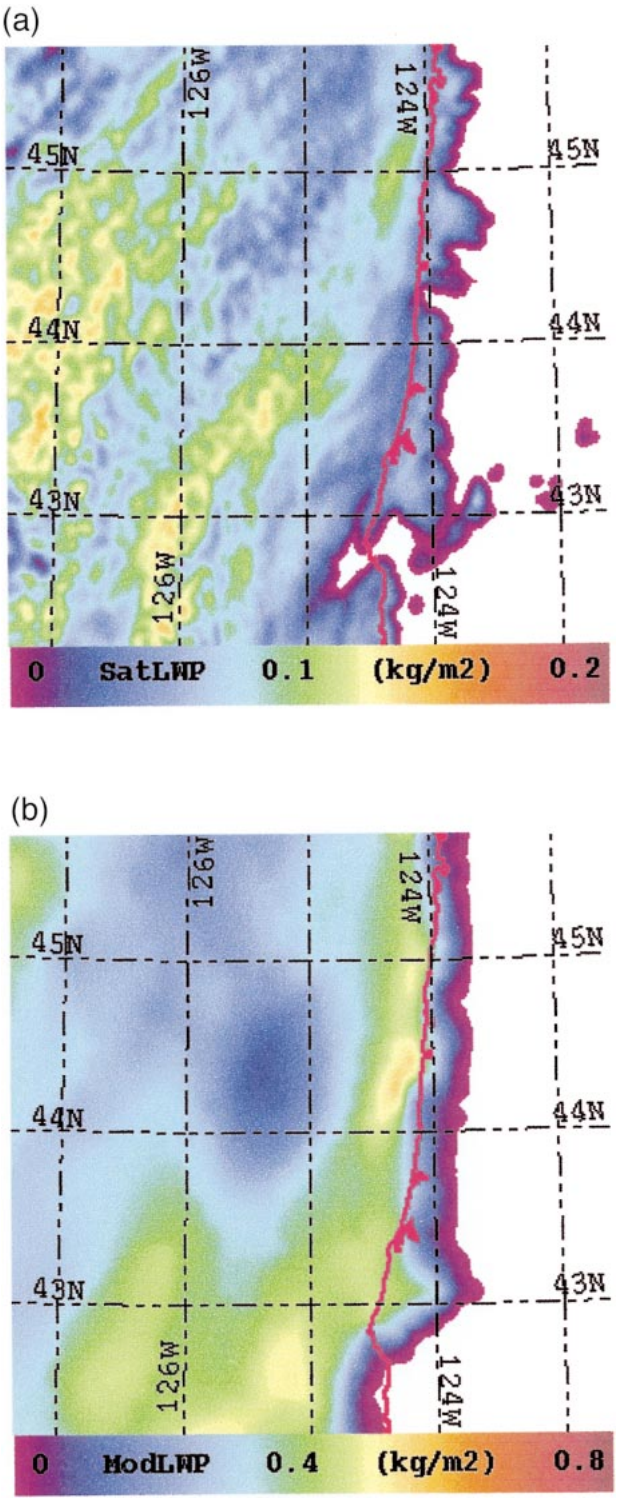

FIG. 9. (a) Satellite-estimated LWP (kg m^{-2}) and (b) COAMPS simulations of LWP (kg m^{-2}) at 1800 UTC 10 Aug for the study region, with graphic overlay of the lat–long grid.

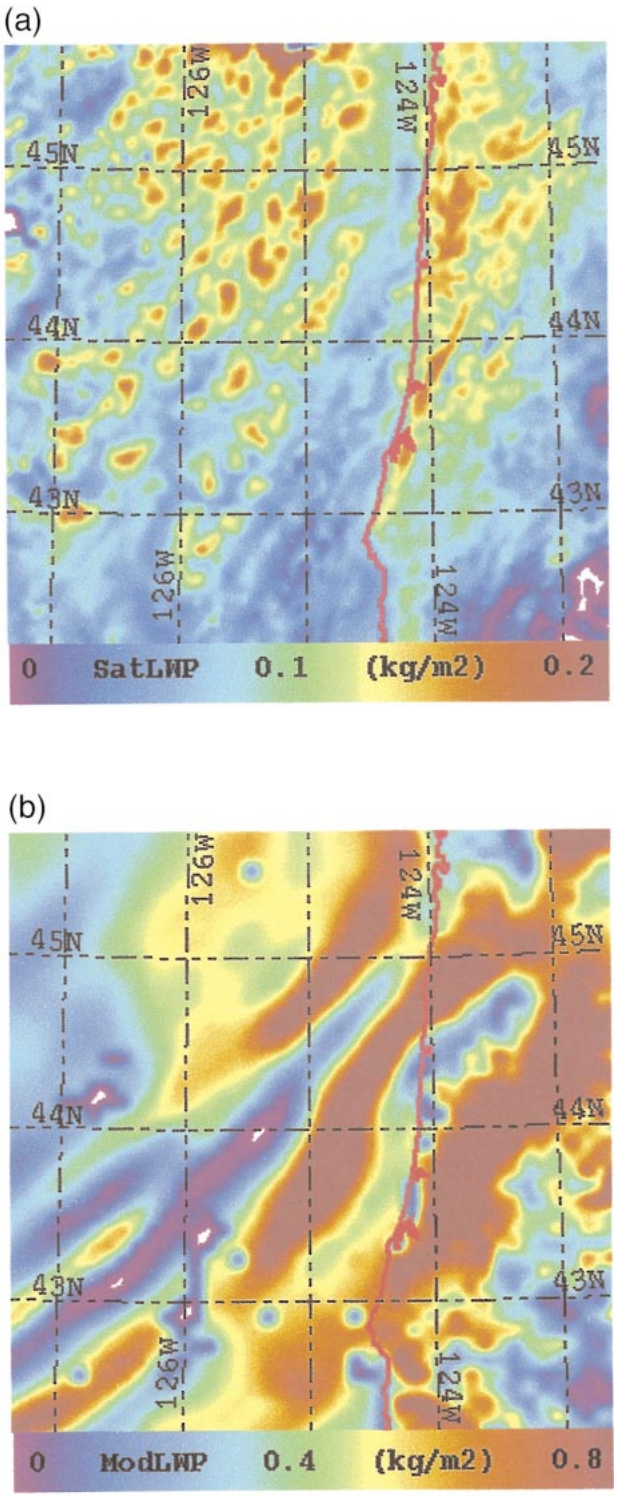

FIG. 10. (a) Satellite-estimated LWP (kg m^{-2}) and (b) COAMPS simulations of LWP (kg m^{-2}) at 1800 UTC 11 Aug for the study region, with graphic overlay of the lat–long grid.

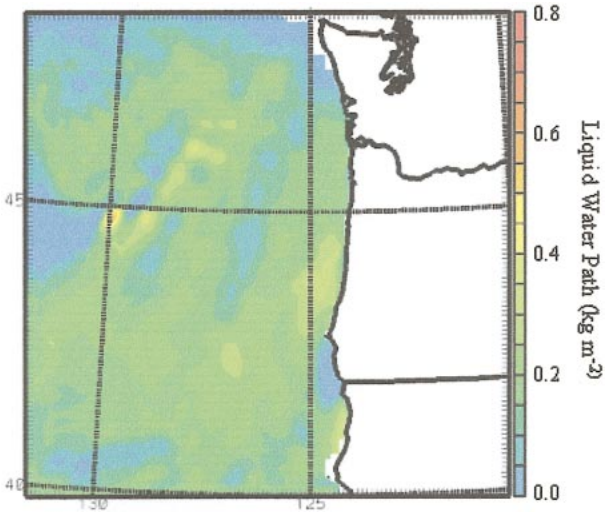

FIG. 11. COAMPS simulation of LWP (kg m^{-2}) at 1800 UTC 10 Aug for a change in the precipitation autoconversion threshold.

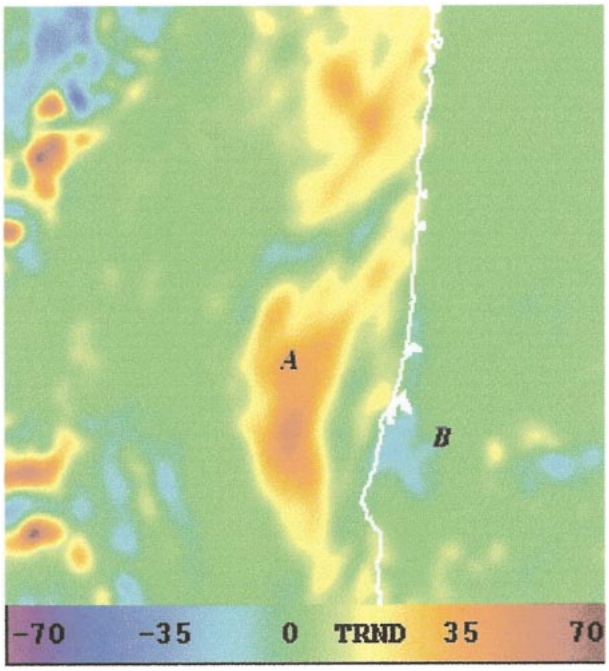

FIG. 12. Temporal trend of LWP (g m^{-2}) for 1600–1800 UTC 9 Aug showing areas of increasing (A) and decreasing (B) values of LWP.

the depth of the cloud layers and the magnitude of the LWP values that developed during the latter 2 days. The diagnosed overestimates in the model-predicted LWP may be caused by inadequate microphysical parameterizations of the model, such as the high threshold (1 g kg^{-1}) for autoconversion from cloud water to rainwater (Kong 1999). The mapped distributions of satellite-derived LWP indicate that modifications to model microphysical parameterization may be necessary. An experimental change in the autoconversion threshold was utilized to test the model sensitivity to this parameter. Figure 11 presents the 1800 UTC forecast on 10 August, corresponding to Fig. 5b but for a COAMPS simulation where the autoconversion threshold was reduced from 1 to 0.5 g kg^{-1}. This change in the threshold parameter caused a substantial reduction in the predicted LWP field. On the other hand, the model results indicated other undesirable effects, including spurious transport of cloud liquid water into the inversion, with resultant evaporative cooling in the inversion and additional deepening of the boundary layer. Thus, additional research is needed to investigate methods for representing the feedbacks between liquid water development, precipitation, and boundary layer convection.

c. Diagnostic products

Satellite multispectral image data are not currently utilized for data assimilation into COAMPS, but a variety of diagnostic procedures can be implemented by combining the satellite and model products for analysis of marine stratus, such as difference fields of model–satellite LWP. Temporal tendencies in satellite-observed parameters have been mapped for the 9–11 August case study. The 2-h tendency of LWP for 9 August (Fig. 12) indicates the location and magnitude of cloud layer evolution. Areas of increasing LWP (location A shown in Fig. 12) during the morning hours help locate areas of enhanced updraft development and cellular structure, while the decreasing LWP, such as that seen in the bay along the central coastline (location B) indicates erosion of the stratus. Tendency fields that indicate an increase in R_e could be used for short-term prediction of drizzle onset. The relationships between drizzle production, R_e, and LWP are being studied using the aircraft microphysical and radar data from this experiment.

The transition in cloud microphysical conditions was also evaluated by study of the cloud condensation nuclei (CCN) spectra and the corresponding mean cloud droplet concentrations during 9–11 August. A variation in the spatial or temporal trend in the satellite-derived effective radius for the cloud layer can be an indication that there has been a change in the microphysical growth processes and/or the concentration of available CCN. This information is valuable for choice of specific parameterizations for aerosol or droplet physics, or in diagnosing electro-optical propagation. The cloud condensation nuclei were sampled using a CCN counter (Vali et al. 1995) at five different supersaturation levels (0.2%–1%). When fit to the $N = CS^k$ form (where N is the CCN concentration, C is a constant representing the number of CCN at 1% supersaturation, S is the supersaturation, and k is the slope parameter), the mean CCN results yielded $N = 630S^{1.4}$ for 9 August, $N = 820S^{0.45}$ for 10 August, and $N = 320S^{0.97}$ for 11 August. Note that these values may be subject to substantial error, as the standard deviations at each supersaturation level were generally between 60% and 70% of the mean.

However, a comparison of the trend in the CCN spectrum characteristics to the trend in mean cloud droplet concentration (N_d) shows agreement, with a decrease in droplet concentrations between 9 August ($N_d = 139 \pm 37$ cm^{-3}) and 11 August ($N_d = 63 \pm 39$ cm^{-3}). Droplet spectra measurements were not available for 10 August. Effective supersaturations were estimated to be 0.3% on 9 August and 0.1% on 11 August. Trends in CCN and cloud droplet concentrations correspond to the transition to a cleaner maritime air mass by 11 August. For the same period, the satellite- and aircraft-derived values of R_e increased from 8 to 16 μm.

Composites of parameters can be produced by averaging parameter values such as R_e at the same time on multiple days, for all days on which each pixel was cloudy and had a retrieved value of that parameter. Such climatologies of satellite-derived microphysical parameters can be extremely useful in classification of meteorological scenarios. For example, comparison of an R_e field with the ''typical'' climatology of cloud droplet size for a given time of day can be applied to model analysis and short-term forecasting of the subsequent cloud layer evolution.

5. Conclusions

Satellite retrievals of cloud droplet effective radius, cloud optical depth, and liquid water path have been used for evaluation of mesoscale model forecasts. Intercomparisons of satellite-derived and aircraft datasets were first employed to validate the satellite retrieval method for LWP. The in situ aircraft data as well as more horizontally extensive satellite retrieval products were then applied to analysis of LWP fields predicted by COAMPS. The 3-day sequences depicting the spatial distributions in cloud and LWP show that the trend toward increasing LWP, deepening cloud layers, and more convective structure was well represented in the model simulations. As the cloud layer evolved, however, COAMPS overpredicted the magnitude of liquid water path, where maximum values of LWP were 3–4 times as large as those indicated from the aircraft data and by the mapped satellite estimates. This degree of overprediction could lead to an extended cloud lifetime that would significantly impact radiative fluxes and diurnal evolution for the marine boundary layer.

The model overprediction of LWP was somewhat improved by changing the number of vertical levels in the simulations from 30 to 45, due to enhancement in the vertical grid resolution both within and above the boundary layer. However, it is not feasible to run the COAMPS model with 45 vertical levels at all times within the current operational scenario. The satellite LWP fields could be used to identify situations where the higher vertical resolution is warranted on a short-term basis.

Analysis of model–satellite LWP differences suggests the need for modifications of COAMPS's current microphysical parameterization. A model experiment in which the liquid water autoconversion threshold was decreased from 1 to 0.5-g kg^{-1} demonstrated improvement in the magnitudes and horizontal distribution of predicted LWP, although it also caused vertical transport of cloud water into the inversion. Research is currently under way to improve both the COAMPS treatment of turbulence in the presence of boundary layer stratus and to modify the microphysical parameterization. Work on the turbulence scheme has resulted in an improvement in the vertical distribution of turbulence intensity. This has the effect of increasing entrainment of dry, potentially warmer air, which reduces the cloud water path. The new microphysics scheme will incorporate drizzle and a more comprehensive treatment of conversion of water species, with methods similar to those of Khairoutdinov and Kogan (2000).

The satellite retrieval methods can provide R_e and LWP fields with a spatial and temporal continuity, which is not available from other sources. Satellite-based analysis of these cloud parameters can also be used to create regional climatologies of cloud layer parameters, and to monitor cloud–aerosol interactions (Wetzel and Stowe 1999). These results additionally provide the rationale for assimilating remotely sensed cloud liquid water path and droplet size into mesoscale models. Such assimilation can improve moisture initialization and cloud physics parameterizations at startup and during model runs.

Acknowledgments. This research was funded by DEPSCoR grants from the Office of Naval Research to DRI (N00014-98-1-0556) and to the University of Wyoming (N00014-97-1-1027). Additional support was provided by a grant to University of Wyoming by the National Science Foundation (ATM 9712859) and a grant to Desert Research Institute from the Office of Naval Research (N000014-01-0295). Two of the authors (WTT and TH) were supported by the Office of Naval Research and the program manager, Naval Research Laboratory, under Program Element 0602435N. Significant participation in the field project and subsequent analysis was supported by the aircraft research group at the University of Wyoming. Many people at the Naval Research Laboratory also contributed to the success of the project, particularly Tom Lee and Joe Turk who made available the real-time and archived satellite data. Collaboration with Roger Samelson, Phillip Barbour, Soline Bielli, and others at Oregon State University with regard to mesoscale modeling and coastal meteorological measurements was extremely beneficial. The authors extend thanks to Hermann Gerber for his collaboration and discussions during the field program.

REFERENCES

Albrecht, B. A., C. S. Bretherton, D. W. Jonson, W. H. Schubert, and A. S. Frisch, 1995: The Atlantic Stratocumulus Transition Experiment—ASTEX. *Bull. Amer. Meteor. Soc.*, **76,** 889–904.

Gerber, H., 1996: Microphysics of marine stratocumulus clouds with two drizzle modes. *J. Atmos. Sci.,* **53,** 1649–1662.

Greenwald, T. J., and S. A. Christopher, 1999: Daytime variation of marine stratocumulus microphysical properties as observed from geostationary satellites. *Geophys. Res. Lett.,* **26,** 1723–1726.

Han, Q., W. B. Rossow, R. M. Welch, A. White, and J. Chou, 1995: Validation of satellite retrievals of cloud microphysics and liquid water path using observations from FIRE. *J. Atmos. Sci.,* **52,** 4183–4195.

Hodur, R. M., 1997: The Naval Research Laboratory's Coupled Ocean/Atmosphere Mesoscale Prediction System (COAMPS). *Mon. Wea. Rev.,* **125,** 1414–1430.

Hogan, T. F., and T. E. Rosmond, 1991: The description of the U.S. Navy Operational Global Atmospheric Prediction System's spectral forecast model. *Mon. Wea. Rev.,* **119,** 1786–1815.

Kaufman, Y. J., and T. Nakajima, 1993: Effect of Amazon smoke on cloud microphysics and albedo—Analysis from satellite imagery. *J. Appl. Meteor.,* **32,** 729–744.

Khairoutdinov, M., and Y. Kogan, 2000: A new cloud physics parameterization in a large-eddy simulation model of marine stratocumulus. *Mon. Wea. Rev.,* **128,** 229–243.

Kong, F., 1999: A study of marine stratus and fog events using COAMPS model. *Third Conf. on Coastal Prediction,* New Orleans, LA, Amer. Meteor. Soc., 1–6.

Lee, T. F., F. J. Turk, and K. Richardson, 1997: Stratus and fog products using *GOES-8–9* 3.9-μm data. *Wea. Forecasting,* **12,** 664–677.

Meier, W. N., J. A. Maslanik, J. R. Key, and C. W. Fowler, 1997: Multiparameter AVHRR-derived products for Arctic climate studies. *Earth Interactions,***1,** 1-005. [Available online at http://Earth Interactions.org.]

Mellor, G. L., and T. Yamada, 1982: Development of a turbulence closure for geophysical fluid problems. *Rev. Geophys. Space Phys.,* **20,** 851–875.

Miller, S. D., 2001: Physical decoupling of the GOES daytime 3.9 μm channel thermal emission and solar reflection components using total solar eclipse. *Int. J. Remote Sens.,* **22,** 9–34.

Minnis, P., P. W. Heck, D. F. Young, C. W. Fairall, and J. B. Snider, 1992: Stratocumulus cloud properties derived from simultaneous satellite and island-based instrumentation during FIRE. *J. Appl. Meteor.,* **31,** 317–339.

Noonkester, V. R., 1984: Droplet spectra observed in marine stratus clouds. *J. Atmos. Sci.,* **41,** 829–845.

Oliver, D. A., W. S. Lewellen, and G. G. Williamson, 1978: The interaction between turbulent and radiative transport in the development of fog and low-level stratus. *J. Atmos. Sci.,* **35,** 301–316.

Paluch, I. R., C. A. Knight, and L. J. Miller, 1996: Cloud liquid water and radar reflectivity of nonprecipitating cumulus clouds. *J. Atmos. Sci.,* **53,** 1587–1603.

Platnick, S., and F. P. J. Valero, 1995: A validation of a satellite cloud retrieval during ASTEX. *J. Atmos. Sci.,* **52,** 2985–3001.

Rutledge, S. A., and P. V. Hobbs, 1983: The mesoscale and microscale structure and organization of clouds and precipitation in midlatitude cyclones. VIII: A model for the ''seeder-feeder'' process in warm-frontal rainbands. *J. Atmos. Sci.,* **40,** 1185–1206.

Stamnes, K., S. C. Tsay, W. Wiscombe, and K. Jayaweera, 1988: Numerically stable algorithm for discrete-ordinate-method radiative transfer in scattering and emitting layered media. *Appl. Opt.,* **27,** 2502–2509.

Tag, P. M., and S. W. Payne, 1987: An examination of the breakup of marine stratus: A three-dimensional numerical investigation. *J. Atmos. Sci.,* **44,** 208–223.

Telford, J. W., and S. K. Chai, 1984: Inversions, and fog, stratus and cumulus formation in warm air over cooler water. *Bound.-Layer Meteor.,* **29,** 109–137.

——, and ——, 1993: Marine fog and its dissipation over warm water. *J. Atmos. Sci.,* **50,** 3336–3349.

Thompson, W. T., S. D. Burk, and J. Rosenthal, 1997: An investigation of the Catalina eddy. *Mon. Wea. Rev.,* **125,** 1135–1146.

Tjernstrom, M., and D. Koracin, 1995: Modeling the impact of marine stratocumulus on boundary layer structure. *J. Atmos. Sci.,* **52,** 863–878.

Wai, M. M. K., 1991: The breakup of marine boundary layer clouds over an inhomogeneous sea-surface temperature field. *Bound.-Layer Meteor.,* **57,** 139–165.

Wetzel, M. A., and T. H. Vonder Haar, 1991: Theoretical development and sensitivity tests of a stratus cloud droplet size retrieval method for AVHRR-K/L/M. *Remote Sens. Environ.,* **36,** 105–119.

——, and L. L. Stowe, 1999: Satellite-observed patterns in stratus microphysics, aerosol optical thickness, and shortwave radiative forcing. *J. Geophys. Res.,* **104,** 31 287–31 299.

——, R. D. Borys, and L. E. Xu, 1996: Satellite microphysical retrievals for land-based fog with validation by balloon profiling. *J. Appl. Meteor.,* **35,** 810–829.

Vali, G., R. D. Kelly, A. Pazmany, and R. E. Macintosh, 1995: Airborne radar and in-situ observations of a shallow stratus with drizzle. *Atmos. Res.,* **38,** 361–380.

——, ——, J. French, S. Haimov, D. Leon, R. E. McIntosh, and A. Pazmany, 1998: Finescale structure and microphysics of coastal stratus. *J. Atmos. Sci.,* **55,** 3540–3564.